# An Improved VMD Method for Use with Acoustic Impact Response Signals to Detect Corrosion at the Underside of Railway Tracks

Yang, Jingyuan; Stewart, Edward; Ye, Jiaqi; Entezami, Mani; Roberts, Clive

[Link to publication on Research at Birmingham portal](#)

*Article*

# An Improved VMD Method for Use with Acoustic Impact Response Signals to Detect Corrosion at the Underside of Railway Tracks

Jingyuan Yang [iD], Edward Stewart, Jiaqi Ye *, Mani Entezami and Clive Roberts [iD]

School of Engineering, University of Birmingham, Birmingham B15 2TT, UK
* Correspondence: j.ye@bham.ac.uk; Tel.: +44-7935431909

**Abstract:** Variational Mode Decomposition (VMD) is widely used for inspection purposes. The initial parameters are usually set manually, which is a limitation of this technique. In this paper, a method to automatically select these parameters through a combination of Singular Value Decomposition (SVD) and Improved-VMD (IVMD) is proposed. VMD is applied multiple times with a varying K-value parameter. The original signal and its sub-signals arising from VMD decomposition are all subjected to SVD. An index representing the relevance between sub-signals and the original signal is obtained by comparing eigenvalues, which are calculated by SVD. The result shows the effectiveness of VMD with different initial K-value parameters. SVD is then further applied to the VMD result for the selected K-value parameter to obtain Shannon entropy, which can be used in the detection and classification of corrosion on the underside of the rail. Comparing with current energy-based methods, the Shannon entropy obtained by IVMD–SVD has the advantage of reducing environmental interference to obtain more uniform energy results. The proposed method can improve the effectiveness of VMD for the impact response signal. The classification of underside corrosion of rails can be realised according to the results obtained from the proposed method.

**Keywords:** impact response signal; VMD; SVD; rail; corrosion inspection; machine learning

## 1. Introduction

Rail corrosion is one of the common faults occurring in plain line railway tracks and has attracted notable attention in recent years [1]. Hernández [2] evaluated the corrosion risk, according to chemical simulation of corrosion formation and propagation at the rail base. Visual inspection techniques are commonly used in corrosion inspection processes [3–6]. However, most inspection focuses on the accessible surfaces of the rail. There are limitations in the current inspection techniques, especially in regard to corrosion of the underside of the rail. For example, it is difficult to detect corrosion through 3D visual inspection where a mapping laser and optical scanner cannot be mapped, due to the location of the fault as it is below the rail and not accessible. Additionally, electromagnetic methods can be limited in extracting information from the underside of the rail where their signals are unable to pass through the whole rail body, due to the skin effect [7] and other attenuation.

In this paper, acoustic inspection is a non-invasive technique that can be used widely and provides accurate results. Acoustic techniques have been used in modern railway inspection, but only in limited applications, such as bearing and gearbox monitoring, in which there has been rapid development in recent years due to the capabilities and effectiveness of acoustic techniques in detecting bearing and gearbox faults in the early stages [8–10]. The sound generated from wheelsets passing through rail discontinuities, such as crossing noses and insulted rail joints (IRJs), can be related to their structural performances, which can potentially be used in fault detection. However, it is challenging to obtain data from vehicles passing damaged rail discontinuities for safety reasons, and, therefore, faulty track pieces have been in laboratory conditions for this kind of inspection.

The signal generated by hammer impact is used for the analysis (impact response signal). This approach has previously been used for classifying faults on railway tracks [11].

Signal decomposition techniques have commonly been used in signal processing methods [8,12–15]. Variational Mode Decomposition (VMD) is a self-adaptive signal de-composition method, proposed in 2014 [16], which has been adopted in inspection applications, particularly for rotational machines. Wang [17] proposed an improved VMD method, by combining VMD with a deep convolutional neural network (DCNN), for the detection of rolling bearing element faults, which enhanced the visibility of the fault feature and, therefore, improved the accuracy of diagnosis. Yi [18] considered the feasibility of extracting fault features from turbine bearings through a combination of VMD and particle swarm optimisation (PSO). This application has the advantage of being able to decompose complicated signals, compared to conventional Empirical Mode Decomposition (EMD). The authors in [19] proposed an application combining VMD and permutation entropy to identify different fault types within bearings with high classification accuracy. Miao [20] considered the application of inspection encoder signals from gearboxes. The signals were decomposed using an advanced VMD method combined with a sparse representation to extract fault information. Miao's proposed method both suppressed noise and enhanced fault impulses. Considering these works, VMD is often applied to signals emanating from rotational machines. However, the features from impact response signals are somewhat different. Considering the feasibility of impact response signals decomposed using VMD, Yang [10] demonstrated that VMD is able to decompose impact response signals from railway tracks with high classification accuracy. However, the faults considered did not include corrosion. This paper, therefore, used VMD for the application of acoustic inspection to the detection and classification of corrosion on the underside of rails.

Previous research indicates that the number of decomposition modes (K-value) is a significant parameter in the performance of VMD. Current research in the selection of the optimal K-value for VMD generally focuses on two aspects. Firstly, the relationship between the original signal and sub-signals, which is known as Instinct Mode Function (IMF). Yang [21] applied kurtosis to develop an indicator for the effect of the relationship on the performance of the VMD algorithm. The improved VMD was then used to detect the early failure of bearings through chatter signals. Li [22] proposed "envelope kurtosis maximum" as an indicator to select the optimal K-value, again by evaluating the relationship between the original signal and sub-signals.

The second popular approach for K-value selection considers the Initial Centre Frequency (ICF) parameter. This approach is suitable for periodic signals, for which it is easy to calculate a centre frequency [16,23]. Jiang [24] proposed an ICF-guide VMD algorithm for extracting minor damage information from bearings.

However, impact response signals are different from the rotational signals considered in the above references. Impact response signals are impulse signals with gradually decreasing energy, differing from rotational signals, which contain a periodic peak in the time domain. Hence, kurtosis-based methods are generally not considered suitable, because of their dependence on the distribution of peaks within the signal. Additionally, it is generally difficult to calculate the centre frequency of non-periodic signals, such as impact response signals. Hence, current techniques for determining K-value are not suitable for selecting the optimal K-value for impact response applications. Therefore, it is necessary to seek an algorithm to select the most suitable decomposed modes for VMD when applied to impact response signals.

In this paper, based on the impact response signal, an improved algorithm for detecting corrosion in the underside of rails is proposed. The algorithm combines VMD, Singular Value Decomposition (SVD), and Shannon entropy techniques. The proposed IVMD–SVD method, through its SVD component, automatically selects the initial parameters for the VMD element. SVD is then further applied to the VMD result to obtain Shannon Entropy, which is used in the detection and classification of underside corrosion. The classification result from a Radial Basis Function (RBF) neural network indicated that the proposed

method could be used in diagnosing underside corrosion. A flow chart describing the structure of the proposed algorithm is provided in Figure 1.
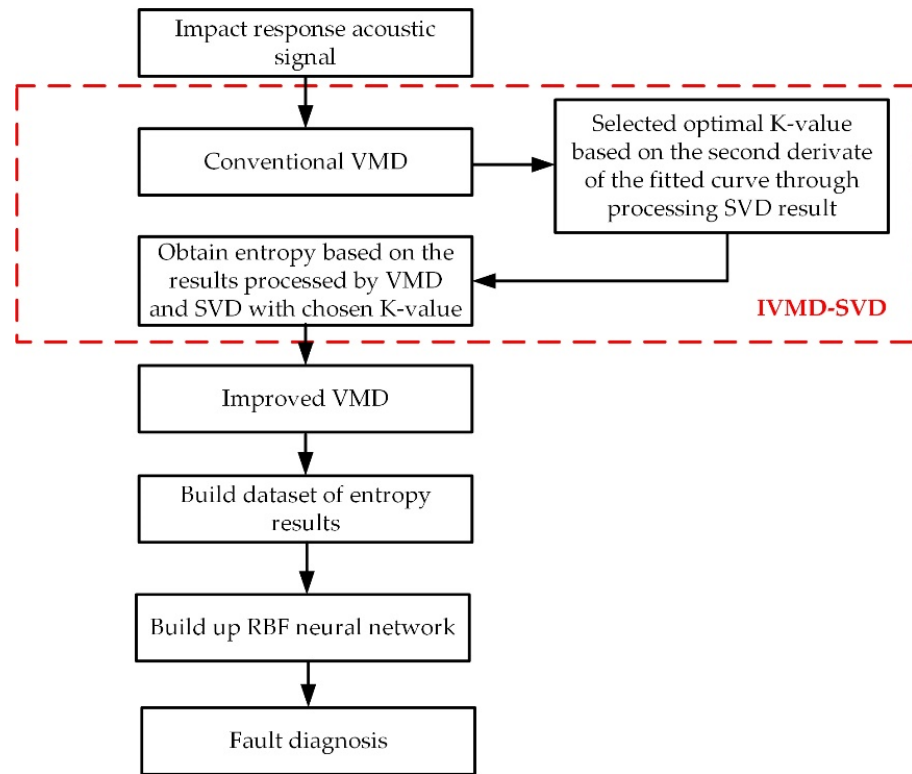


**Figure 1.** Flow chart indicating underside corrosion diagnosis method.

## 2. Decomposition Methodology

### 2.1. Brief Introduction to VMD

VMD is a self-adaptive and non-recursive signal decomposition method based on Wiener filtering, Hilbert transform, and frequency distortion [21]. The principle of the VMD algorithm is to decompose components of a signal into different adaptive bands for the development of a generalised Wiener filter. The input signal is decomposed into limited bandwidth modes, $u_k$, with each sub-signal tightly focused around its own central frequency. The bandwidth of each mode can be evaluated by solving the constrained variational problem shown in Equation (1) [21].

$$\min_{\{u_k\},\{\omega_k\}} \left\{ \sum_k \| \alpha_t \left[ \left( \delta(t) + \frac{j}{\pi t} \right) * u_k(t) \right] exp^{-j\omega kt} \|_2^2 \right\} m$$
$$s.t. \sum_k u_k = f \tag{1}$$

where $\delta$ is the Dirac distribution; $k$ is the number of the mode. $u_k$ are the set of all modes; and $\omega_k$ is the centre frequency of each mode.

In order to remove constraints on Equation (1), the constrained variational problem can be solved considering a Lagrangian multiplier $\lambda(t)$ and a quadratic penalty term $\alpha$, which results in Lagrangian $\mathcal{L}$, as shown in Equation (2):

$$\mathcal{L}(\{u_k\},\{\omega_k\},\lambda) = \alpha \sum_k \left\{ \sum_k \| \partial_t \left[ \left( \delta(t) + \frac{j}{\pi t} \right) * u_k(t) \right] exp^{-j\omega kt} \|_2^2 \right\} + \| f(t) - \sum_k u_k(t) \|_2^2$$
$$+ \left\langle \lambda(t), f(t) - \sum_k u_k(t) \right\rangle \tag{2}$$

In order to obtain an optimal solution of the constrained variational model, the Alternative Direction Method of Multipliers (ADMM) is applied to solve Equation (2). Hence,

the mode $u_k$ and centre frequency $\omega_k$ can be updated, as shown in Equations (3) and (4), respectively:

$$u_k^{n+1} \overset{\circ\circ}{\leftarrow} \underset{u_k}{argmin} L\left(\left\{u_{i<k}^{n+1}\right\}, \left\{u_{i\geq k}^{n+1}\right\}, \left\{\omega_i^{n+1}\right\}, \lambda^n\right) \tag{3}$$

$$\omega_k^{n+1} \overset{\circ\circ}{\leftarrow} \underset{u_k}{argmin} L\left(\left\{u_i^{n+1}\right\}, \left\{u_{i<k}^{n+1}\right\}, \left\{\omega_{i\geq k}^{n+1}\right\}, \lambda^n\right) \tag{4}$$

Decomposition to identify all sub-signals (IMFs) can be achieved through continuous iteration as presented in Equation (5):

$$\overset{\wedge}{u}_k{}^{n+1}(\omega) = \frac{\overset{\wedge}{f}(\omega) - \sum_{i<k} \overset{\wedge}{u}_i{}^{n+1}(\omega) + \frac{\overset{\wedge}{\lambda}{}^n(\omega)}{2}}{1 + 2\alpha\left(\omega - \omega_k^n\right)^2} \tag{5}$$

### 2.2. Brief Introduction to SVD

Singular Value Decomposition (SVD) is an algorithm based on an orthogonal matrix transformation. The matrix $A(m \times n)$, when processed by SVD, can be decomposed into three matrices with different dimensions, as shown in Equation (6):

$$A = USV^T \tag{6}$$

where $U = [u_1, u_2, \ldots, u_1] \in R^{m \times m}$ and $V = [v_1, v_2, \ldots, v_1] \in R^{n \times n}$. The notation $S$ is a diagonal matrix with n singular values with descending order, showing as $S = [diag(\lambda_1, \lambda_2, \ldots, \lambda_n), 0] \in R^{m \times n}$. Singular values from $S$ contain the information from the original signal.

### 2.3. IVMD–SVD

The proposed IVMD–SVD method uses an algorithm to automatically select the number of modes (K-values) to be used in the decomposition of the impact response signal. The result, decomposed by the selected modes, is processed to obtain the Shannon entropy, which is then used in further analysis.

The appropriate K-value is selected through consideration of the relationship between IMFs (sub-signals) and the original signal. First, SVD is used to obtain eigenvalues from both the IMFs and the original signal. Then, the ratio between eigenvalues of each IMF and the original signal is calculated. This ratio is then used as an index in the evaluation of the relationship between sub-signals and the original signal. This evaluation process selects the optimal K-value, and, hence, the number of modes to be used in the decomposition of the response signal. The process for selecting the optimal K-value is described in the following section.

The mechanism by which the optimal K-value is selected is summarised in Figure 2.

The steps indicated in Figure 2 are as follows:

Step 1: Sub-signals, $IMF_i(t)$, are obtained by performing VMD using a range of K-values from 2 to $N$, i.e., VMD ($i = 1, 2, \ldots, N$).

Step 2: The IMFs calculated from each VMD are combined to form Hankel matrix representations [25] of each sub-signal using a phase–space reconstruction process, as shown in Equation (7).

$$X = \begin{pmatrix} IMF_{i1} & IMF_{i2} & & IMF_{in} \\ IMF_{i2} & IMF_{i3} & \cdots & IMF_{i(n-1)} \\ & \vdots & \ddots & \vdots \\ IMF_{i(m-n+1)} & IMF_{i(m-n+2)} & \cdots & IMF_{im} \end{pmatrix} \tag{7}$$

where $m$ is the sample number of the signal, and $n$ is the dimension of the matrix.

Step 3: Eigenvalues are calculated for each Hankel matrix IMF representation using SVD, as shown in Equation (8).

$$SVD(IMF_i(t)) \Rightarrow \begin{pmatrix} \lambda_{i1} & 0 & 0 \\ 0 & \ddots & 0 \\ 0 & 0 & \lambda_{ik} \end{pmatrix} \tag{8}$$
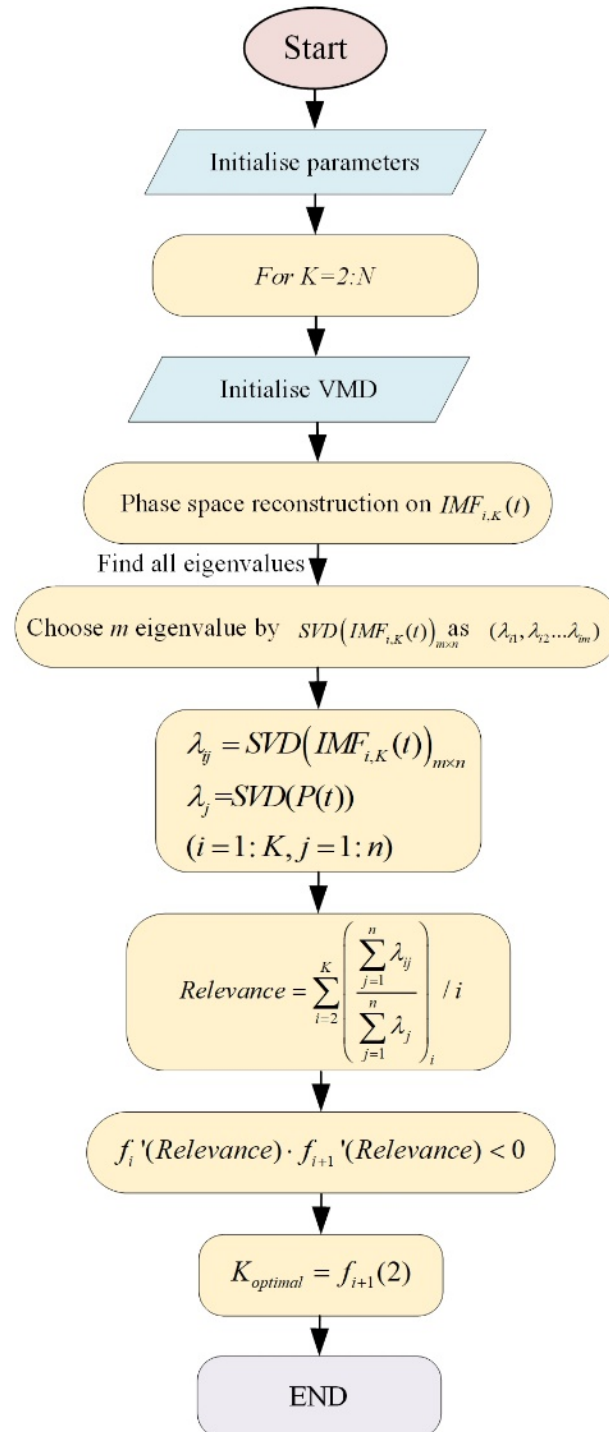


**Figure 2.** Process of selecting optimal K-value.

At this stage, the original signal is also converted to a Hankel matrix representation and SVD is applied, as shown in Equation (9):

$$SVD((F(t)) \Rightarrow \begin{pmatrix} \lambda_1 & 0 & 0 \\ 0 & \ddots & 0 \\ 0 & 0 & \lambda_k \end{pmatrix} \tag{9}$$

The $\{Ratio\}_i$ defined in Equation (10), represents the relationship between each sub-signal and the original signal.

$$\{Ratio\}_i = \left( \frac{\sum_{j=1}^k \lambda_{ij}}{\sum_{j=1}^k \lambda_j} \right) = \begin{pmatrix} Ratio_{12} & Ratio_{13} & \dots & Ratio_{1N} \\ Ratio_{22} & Ratio_{23} & \ddots & Ratio_{2N} \\ & Ratio_{33} & & \vdots \\ & & & Ratio_{NN} \end{pmatrix} \tag{10}$$

As the number of IMFs and, thus, *ratios* vary with K-value, the mean *ratio* (*Relevance*) is calculated to allow direct comparison. *Relevance* is a single measure of the relationship between the original signal and all of its sub-signals. It is generated for each K-value. This is shown in Equation (11):

$$Relevance = \sum_{i=2}^N \{ratio\}_i / i \tag{11}$$

Step 4: The *Relevance* obtained from different K-values can be plotted to form a curve. The second derivative is applied to this curve in the evaluation of the optimal K-value. The optimal value is selected at the point of inflection above a specified threshold. An example is presented in Section 3.

*2.4. Feature Extraction*

Having used the IVMD approach to identify the optimal K-value, a process using the selected K-value is then applied to achieve fault detection. VMD is performed using the selected K-value to generate IMFs and SVD is then applied to generate eigenvalues for each IMF, followed by filtering to generate Shannon entropy, which is then used for fault detection. The process of using the eigenvalues is as follows.

Each eigenvalue is divided by the sum of the eigenvalues for a particular IMF to obtain a set of ratio results. The first $l$ eigenvalues are selected, based on evaluating the value of the ratio against a threshold $a$ to eliminate redundant information. The process is shown in Equation (12):

$$\sum_{j=1}^l \lambda_{ij} / \sum_{j=1}^g \lambda_{ij} > a \tag{12}$$

where $g$ is the total number of eigenvalues. The total value of first $l$ eigenvalues is then used to calculate the Shannon entropy which is used in fault detection. By defining $p_{ij} = \lambda_{ij} / \sum_{j=1}^l \lambda_{ij}$, the Shannon entropy of each IMF is calculated, using Equation (13):

$$E_i = \sum_{j=1}^l p_{ij} \log p_{ij} \tag{13}$$

The Shannon entropies from all IMFs can be combined, as shown in Equation (14), for use in fault diagnosis:

$$E = [E_1, E_2, \dots, E_i] \tag{14}$$

### 3. Experimentation and Analysis

#### 3.1. Laboratory Testing

In order to demonstrate the decomposition methodology described above, and to investigate how impact response signals vary in the presence of underside corrosion, a series of laboratory-based experiments were undertaken. A National Instrument (NI) device was used to collect the signals. Different depths of artificial defects were created in two rail sections, based on a railway maintenance standard [26], while a third rail section was kept as a healthy rail sample. Details of the artificial defects are shown in Figure 3 and described in Table 1.
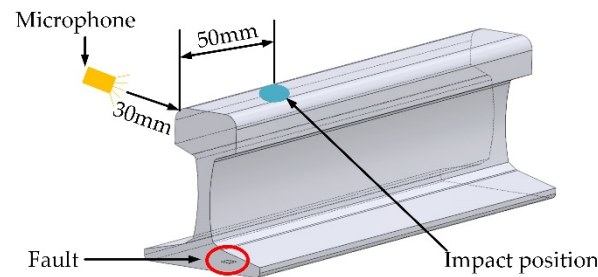


**Figure 3.** Geometry of artificial corrosion.

**Table 1.** Artificial corrosion geometry.

| Depth | Area | Position |
|---|---|---|
| 0.1 mm<br>0.75 mm | 6 mm × 6 mm | 50 mm from the rail end |

The impact response acoustic signal generated by striking the healthy rail sample in the location indicated in Figure 3 is shown in the time and frequency domains in Figure 4.
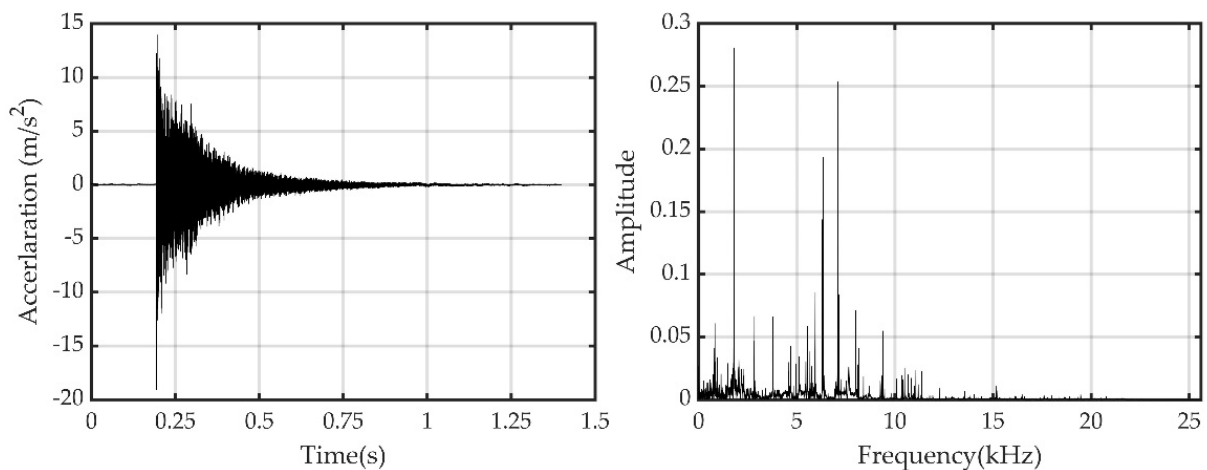


**Figure 4.** Acoustic impact response signal.

As described above, the IVMD–SVD algorithm was used to decompose the experimental signals. Initially K-values of 3 to 12 were used in the analysis.

To demonstrate the procedure for the selection of the optimal K-value, a curve obtained from the relationship between IMFs generated using IVMD–SVD and the original signal was used, and the curve is shown in Figure 5.
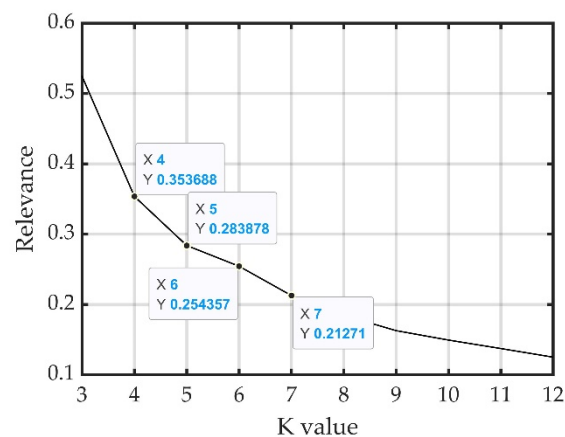
**Figure 5.** Optimal K-value selection from the acoustic impact response signal.

The curve in Figure 5 shows a general downtrend. If the K-value was large, the sub-signals from the higher numbered decomposed modes were generally less relevant to the original signal. Conversely, if the K-value was too small, useful information might be excluded. The preferred K-value occurred at the first point of significant inflection in the curve. This was identified by observing the sign and the difference in values of the second derivative of the curve. The difference in values should be at least 0.05, as identified in [16].

Using the example in Figure 5, the values of the second derivative at K-value 5, and K-value 6 were 0.0403 and −0.0121, respectively. The product of these two values was negative. The absolute difference was larger than 0.05. Hence, the optimal K-value was chosen to be K = 6.

### 3.2. Result Analysis

The result of Shannon entropy was then obtained using IVMD–SVD with the selected K-value. The process was applied to 30 measurements of each of the three rail conditions presented in Figure 6. The blue, red, and yellow bars represent healthy, 0.1 mm, and 0.75 mm depths of fault, respectively.
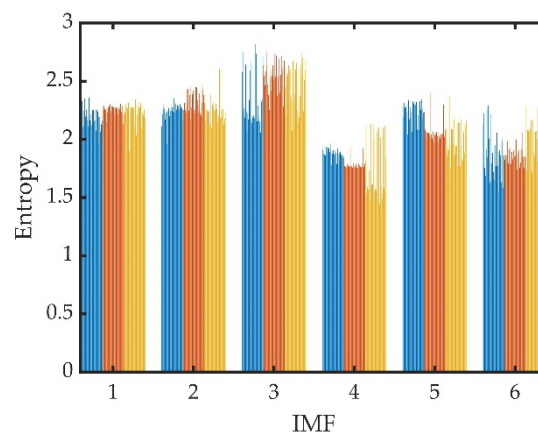


**Figure 6.** Entropy results from IVMD-SVD.

In order to evaluate the effectiveness of IVMD–SVD it was compared to the energy ratio, which is a classic energy-based method [27]. The approach is based on the sum of the

energy from the original signal considered in the frequency domain. The energy ratio was calculated as the ratio between each IMF and the total energy, as shown in Equation (15):

$$
\begin{aligned}
E_i &= \sum |IMF_i(t)|^2 (i = 1, 2, \ldots, m) \\
E &= \sum_{i=1}^{m} E_i \\
p_i &= E_i / E
\end{aligned}
\tag{15}
$$

The comparison of results from the Shannon entropy obtained from IVMD–SVD and the energy ratio methods are shown in Figure 7.
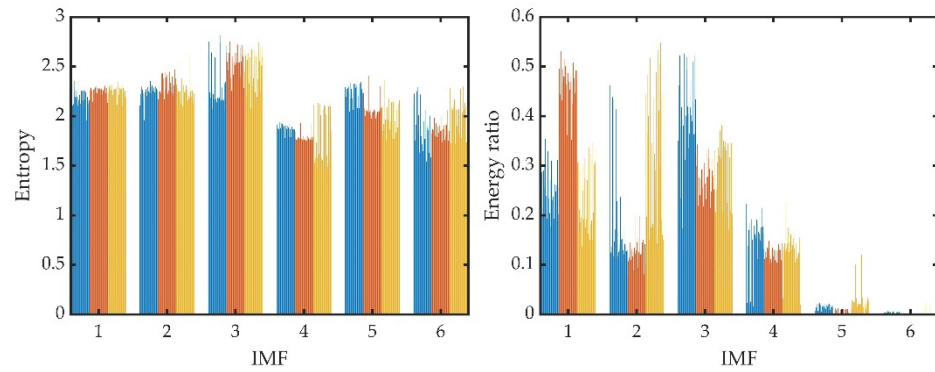


**Figure 7.** Comparison of results obtained using the IVMD–SVD and energy ratio methods.

The statistical parameter Distinction degree (*D*) was used to evaluate the uniformity of the distribution of energy-based results obtained for the same rail conditions. Firstly, considering each rail condition, each entropy in each IMF ($E_{ij}$) was divided by the mean value of all entropies to obtain a set of ratios ($R_{ij}$), using Equation (16):

$$
R_{ij} = E_{ij} / \left( \sum_{j=1}^{z} E_{ij} / z \right)
\tag{16}
$$

where *z* is the number of signals obtained from a particular rail condition.

Secondly, the absolute difference ($D_i$) between each two adjacent ratios ($R_{ij}$ and $R_{i(j+1)}$) was calculated. Then, the distinction degree (*D*) was obtained by summing these differences ($D_i$) as in Equation (17):

$$
D_i = \sum_{j=1}^{z} \left| R_{ij} - R_{i(j+1)} \right|
\tag{17}
$$

Finally, the set of distinction degrees including all IMFs was represented as Equation (18):

$$
D = [D_1, D_2, \ldots, D_i]
\tag{18}
$$

A comparison of the distinction degree obtained using the two energy-based methods is shown in Figure 8.
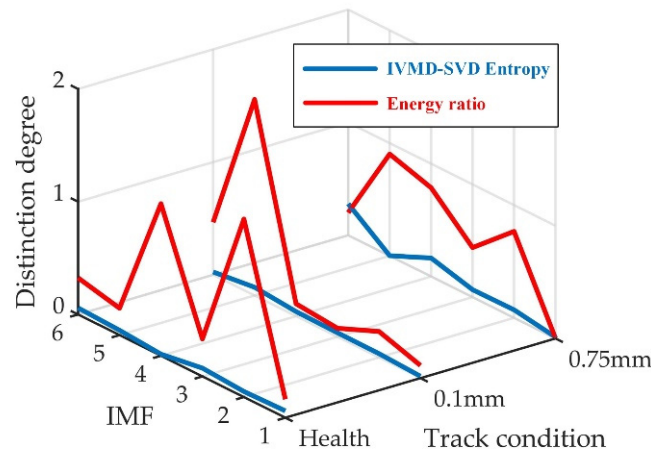
**Figure 8.** Comparison of distinction degrees between two methods for acoustic signals.

Figure 8 shows that, for all health conditions, the average distinction degree obtained from the entropy result was lower than that obtained using the energy ratio. This indicated that the entropy results processed using IVMD–SVD were more uniform than those obtained using the energy ratio method. The proposed method was, therefore, considered more robust against environmental interference, such as that caused by a change of impact location or force.

In order to further validate the effectiveness of the IVMD–SVD algorithm, the evaluation process was repeated using vibration-based impact response signals. A vibration-based impact response signal is another impact response signal closely related to acoustic signals.

The optimal K-value selection from the vibration-based impact response signals is shown as Figure 9. The products of the second derivatives at K-value 5 (−0.038) and K-value 6 (0.019) were negative. The absolute difference of these two second derivatives was 0.057 which was larger than the threshold of 0.05. This indicated that the optimal K-value was 6, which was the same as the conclusion drawn for the acoustic version of the impact response signal.
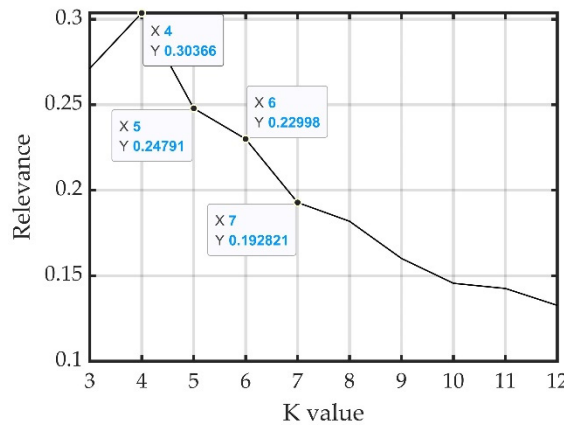


**Figure 9.** Comparison of distinction degrees between two methods for vibration signals.

The distinction degree results from IVMD–SVD entropy and energy ratio are presented in Figure 10.
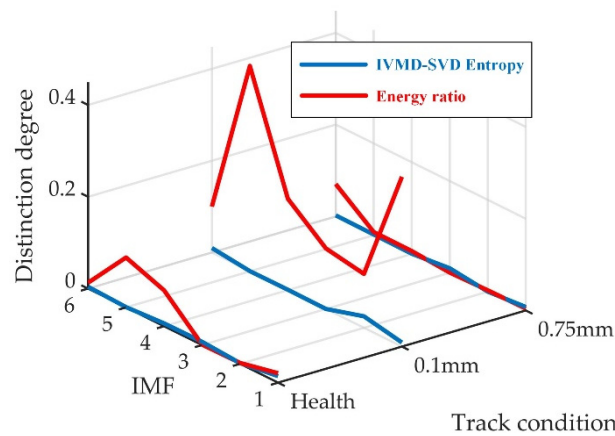
**Figure 10.** Comparison of distinction degrees between two methods for acoustic signals.

The result for the vibration-based signal presented in Figure 10 was similar to that obtained from the acoustic signal. The distinction degree values calculated from IVMD–SVD were lower than those calculated from the energy ratio. Therefore, it was further demonstrated that IVMD–SVD produced more uniformly decomposed signals, and that there was consistency when applied to both acoustic and vibration-based signals. Hence, it was considered that the approach was suitable for reducing environmental effects in a range of recorded signals.

To illustrate the effectiveness of appropriately selecting the K-value on fault classification, an index representing the capacity for identification ($C_k$) of different rail conditions was calculated. The index could be described as a subtraction of the maximum and minimum differences from the mean value of entropy [10], as given in Equation (19).

$$
\begin{aligned}
c_{max\ i} &= max\left|\overline{C_i} - E_{ij}\right| \\
c_{min\ i} &= min\left|\overline{C_i} - E_{ij}\right| \\
C_k &= \sum_{i=1}^{K}\left|c_{max\ i} - c_{min\ i}\right|
\end{aligned}
\tag{19}
$$

where the $\overline{C_i}$ is the mean value of $IMF_i(t)$. The identification capacity index results for each K-value, generated for the acoustic impact response signals, are shown in Figure 11.
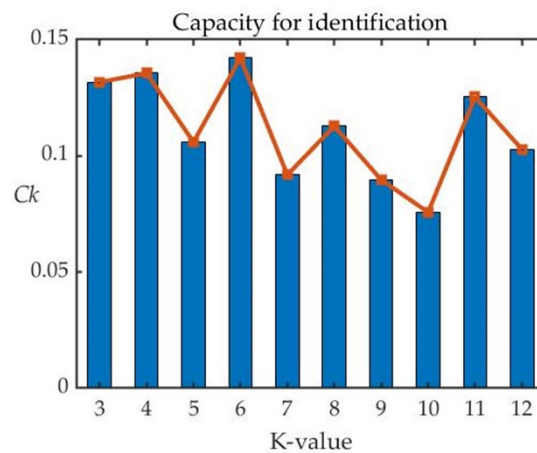


**Figure 11.** Capacity for identification.

The values presented in Figure 11 represent the differences in signals obtained from different rail conditions, considered by K-value used in the processing. The effect of the signal decomposition was better when the value of $C_k$ was higher. The figure shows that

the highest value of $C_k$ corresponded to K = 6. This further demonstrated that the selected K-value was the most appropriate in differentiating the different rail conditions.

This section demonstrated that the proposed method was suitable for the differentiation of rail conditions. The following section explores how the approach can be used to develop a fault classification system, based on acoustic impact response signals.

### 3.3. Fault Classification

To evaluate the effectiveness of the proposed algorithm for fault classification, the experimental signals were decomposed using VMD with different K-values (3 to 12). The entropy results from the different VMD applications were used as the dataset for an RBF neural network, which was used to identify the health condition of the rail.

Example results for classification accuracy and the confusion matrix are presented in Figures 12 and 13. The results shown in the figures are for the selected K-value, K = 6.
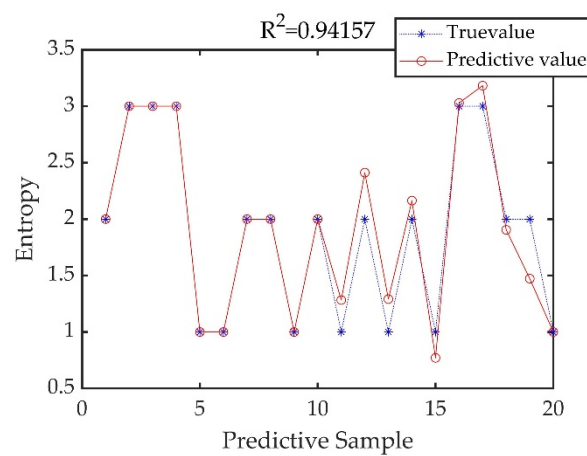


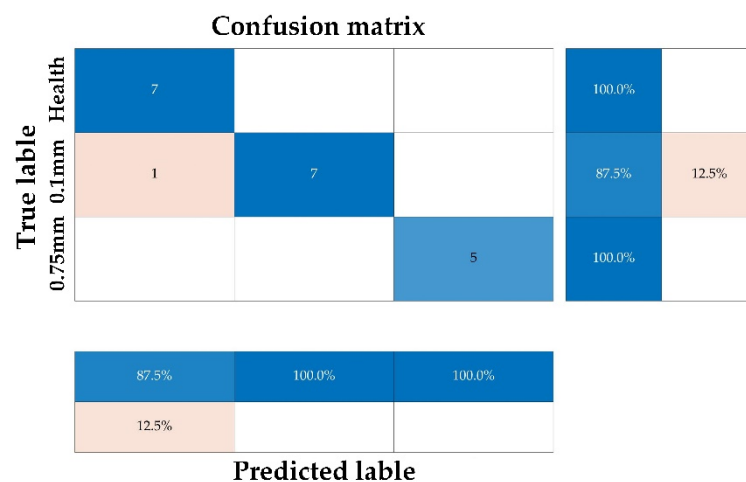**Figure 12.** Accuracy of RBF.



**Figure 13.** Confusion matrix of RBF.

The two figures show that, for the selected K-value, both healthy and faulty rails could be classified with over 94% accuracy. This suggested that acoustic impact response signals obtained from different rail conditions could be effectively classified using the proposed IVMD–SVD method. All healthy and all 0.75 mm samples were identified correctly. One 0.1 mm sample (12.5%) was incorrectly identified as healthy. However, this was considered to be due to the small size of the defect, which might also have been too small to diagnose using existing approaches.

The accuracy results for the different K-values (3–12) are shown in Table 2 and Figure 14.

**Table 2.** Accuracy results for different K-values.

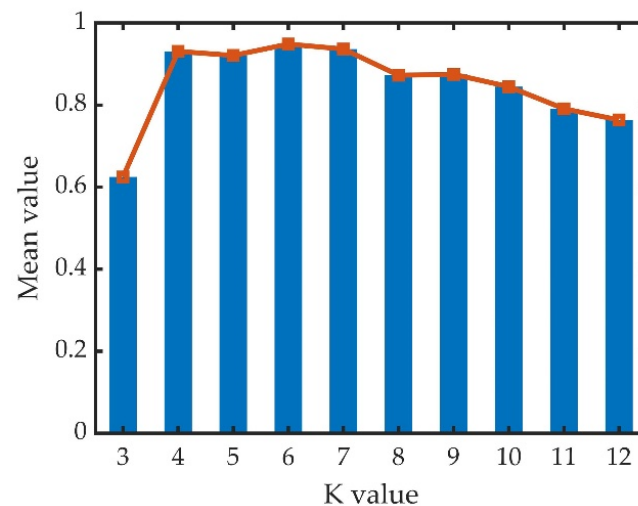| K-Value | Accuracy |
|---------|----------|
| 3 | 0.625 |
| 4 | 0.931 |
| 5 | 0.921 |
| 6 | 0.949 |
| 7 | 0.936 |
| 8 | 0.873 |
| 9 | 0.875 |
| 10 | 0.845 |
| 11 | 0.791 |
| 12 | 0.764 |



**Figure 14.** Accuracy results for different K-values.

The figure suggests that it was difficult to classify signals when K = 3, which had only around 60% accuracy. The highest accuracy was achieved when K = 4 to 7 with the absolute greatest accuracy occurring for K = 6.

Hence, it was demonstrated that the value of K = 6, automatically selected by the proposed IVMD–SVD process, had the greatest effectiveness in decomposition of acoustic impact response signals for use in fault classification. Furthermore, it was demonstrated that underside corrosion of the rail could be effectively diagnosed using the IVMD–SVD method.

## 4. Conclusions

In this paper, a novel algorithm (IVMD–SVD) was proposed to automatically select the initial parameters for use in the VMD algorithm. Shannon entropy obtained from the proposed IVMD–SVD was used to categorise the significance of rail base corrosion.

The statistical parameter distinction degree was used to compare the uniformity of distribution of both energy-based results obtained for particular rail conditions. Compared with the energy ratio results, the proposed entropy-based method was more robust regarding environmental interference, such as that caused by a change of impact location or force.

A further index, based on maximum and minimum differences from the mean value, was applied to evaluate the capacity for identification of different track conditions. It

demonstrated that using the proposed method to select the K-value allowed effective identification of track conditions and faults from acoustic impact response signals.

An RBF neural network was then used for fault classification. The results showed that the proposed method could effectively classify signals from different rail conditions and that the effectiveness was maximised when using the automatically selected K-value.

In conclusion, this paper describes a new method (IVMD–SVD) and demonstrates its particular effectiveness in extraction of features from impact response signals. The proposed method efficiently selects the optimal K-value to be used in the initialisation of the VMD algorithm, thereby maximising its effectiveness for the decomposition of impact response signals. Furthermore, the results obtained from the algorithm were shown to be effective in the identification and classification of different extents of rail corrosion.

Additionally, some work needs to be completed in the future. Firstly, the size of the dataset needs to be expanded. Secondly, the current algorithm is only specifically used for the impact response signal. The effectiveness of the proposed method on other signals needs further research.

**Institutional Review Board Statement:** Not applicable.

**Informed Consent Statement:** Not applicable.

**Data Availability Statement:** All relevant data are shown in the paper or could be recreated by following the methodology in the paper.

**Conflicts of Interest:** The authors declare no conflict of interest.

## References

1. Board, T.R. *Rail Base Corrosion Detection and Prevention*; The National Academies Press: Washington, DC, USA, 2007.
2. Hernandez, F.C.R.; Plascencia, G.; Koch, K. Rail base corrosion problem for North American transit systems. *Eng. Fail. Anal.* **2009**, *16*, 281–294. [CrossRef]
3. Ye, J.Q.; Stewart, E.; Zhang, D.C.; Chen, Q.Y.; Roberts, C. Method for automatic railway track surface defect classification and evaluation using a laser-based 3D model. *Iet Image Process.* **2020**, *14*, 2701–2710. [CrossRef]
4. Zhan, Y.; Dai, X.X.; Yang, E.H.; Wang, K.C.P. Convolutional neural network for detecting railway fastener defects using a developed 3D laser system. *Int. J. Rail Transp.* **2021**, *9*, 424–444. [CrossRef]
5. Ye, J.Q.; Stewart, E.; Roberts, C. Use of a 3D model to improve the performance of laser-based railway track inspection. *Proc. Inst. Mech. Eng. Part F J. Rail Rapid Transit* **2019**, *233*, 337–355. [CrossRef]
6. Zhang, Z.; Liang, M.; Liu, Z. A Novel Decomposition Model for Visual Rail Surface Inspection. *Electronics* **2021**, *10*, 1271. [CrossRef]
7. Sophian, A.; Tian, G.Y.; Fan, M.B. Pulsed Eddy Current Non-destructive Testing and Evaluation: A Review. *Chin. J. Mech. Eng.* **2017**, *30*, 500–514. [CrossRef]
8. Zhang, D.C.; Yu, D.J. Multi-fault diagnosis of gearbox based on resonance-based signal sparse decomposition and comb filter. *Measurement* **2017**, *103*, 361–369. [CrossRef]
9. Zhang, D.C.; Entezami, M.; Stewart, E.; Roberts, C.; Yu, D.J. Adaptive fault feature extraction from wayside acoustic signals from train bearings. *J. Sound Vib.* **2018**, *425*, 221–238. [CrossRef]
10. Pan, A.X.; Yang, Z.G. Cause analysis and countermeasure on premature failure of a driven gear for the high-speed train. *Eng. Fail. Anal.* **2022**, *139*, 106487. [CrossRef]
11. Yang, J.Y.; Stewart, E.; Entezami, M. Decomposition methods for impact-based fault detection algorithms in railway inspection applications. *IET Signal Process.* **2022**, *16*, 935–944. [CrossRef]
12. Shiri, H.; Wodecki, J.; Ziętek, B.; Zimroz, R. Inspection Robotic UGV Platform and the Procedure for an Acoustic Signal-Based Fault Detection in Belt Conveyor Idler. *Energies* **2021**, *14*, 7646. [CrossRef]

13.  Zhao, S.X.; Zhang, J.M.; Xu, L.Y.; Chen, X.L. Combine harvester assembly fault diagnosis based on optimized multi-scale reverse discrete entropy. *Trans. Can. Soc. Mech. Eng.* **2021**, *46*, 1–16. [CrossRef]

14.  Nishat Toma, R.; Kim, C.-H.; Kim, J.-M. Bearing Fault Classification Using Ensemble Empirical Mode Decomposition and Convolutional Neural Network. *Electronics* **2021**, *10*, 1248. [CrossRef]

15.  Sun, Y.K.; Cao, Y.; Li, P. Fault diagnosis for train plug door using weighted fractional wavelet packet decomposition energy entropy. *Accid. Anal. Prev.* **2022**, *166*, 106549. [CrossRef] [PubMed]

16.  Dragomiretskiy, K.; Zosso, D. Variational Mode Decomposition. *Ieee Transactions on Signal Processing* **2014**, *62*, 531–544. [CrossRef]

17.  Wang, R.; Xu, L.; Liu, F.K. Bearing fault diagnosis based on improved VMD and DCNN. *J. Vibroengineering* **2020**, *22*, 1055–1068. [CrossRef]

18.  Yi, C.C.; Lv, Y.; Dang, Z. A Fault Diagnosis Scheme for Rolling Bearing Based on Particle Swarm Optimization in Variational Mode Decomposition. *Shock. Vib.* **2016**, *2016*, 1–10. [CrossRef]

19.  An, X.L.; Pan, L.P. Bearing fault diagnosis of a wind turbine based on variational mode decomposition and permutation entropy. *Proc. Inst. Mech. Eng. Part O-J. Risk Reliab.* **2017**, *231*, 200–206. [CrossRef]

20.  Miao, Y.H.; Zhao, M.; Yi, Y.G.; Lin, J. Application of sparsity-oriented VMD for gearbox fault diagnosis based on built-in encoder information. *Isa Trans.* **2020**, *99*, 496–504. [CrossRef]

21.  Yang, K.; Wang, G.F.; Dong, Y.; Zhang, Q.B.; Sang, L.L. Early chatter identification based on an optimized variational mode decomposition. *Mech. Syst. Signal Pr.* **2019**, *115*, 238–254. [CrossRef]

22.  Li, H.; Liu, T.; Wu, X.; Chen, Q. An optimized VMD method and its applications in bearing fault diagnosis. *Measurement* **2020**, *166*, 108185. [CrossRef]

23.  Liu, H.D.; Li, D.Y.; Yuan, Y.; Zhang, S.J.; Zhao, H.M.; Deng, W. Fault Diagnosis for a Bearing Rolling Element Using Improved VMD and HT. *Appl. Sci.-Basel* **2019**, *9*, 1439. [CrossRef]

24.  Jiang, X.X.; Shen, C.Q.; Shi, J.J.; Zhu, Z.K. Initial center frequency-guided VMD for fault diagnosis of rotating machines. *J. Sound Vib.* **2018**, *435*, 36–55. [CrossRef]

25.  Zhao, M.; Jia, X.D. A novel strategy for signal denoising using reweighted SVD and its applications to weak fault feature enhancement of rotating machinery. *Mech. Syst. Signal Pr.* **2017**, *94*, 129–147. [CrossRef]

26.  Board, T.R. *Guidelines for Rail Base Inspection and Rail Condemnation Limits for Corrosion-Induced Material Loss*; The National Academies Press: Washington, DC, USA, 2009.

27.  Sun, Z.Q.; Zhang, H.J. Application of empirical mode decomposition based energy ratio to vortex flowmeter state diagnosis. *J. Cent. South Univ. Technol.* **2009**, *16*, 154–159. [CrossRef]